

Effects of Energetic Polymers on Laser Photothermal Imaging Materials

S. G. Koulikov and Dana D. Dlott[▲]

Department of Chemistry, University of Illinois at Urbana-Champaign, Urbana, Illinois

The effects of adding a thin layer of an energetic polymer such as nitrocellulose (NC) to laser photothermal imaging media are investigated. Photothermal media are used which are model systems for computer-to-plate or computer-to-press imaging. The media consist of a substrate, a thin absorbing metallic absorbing layer and a silicone rubber imaging layer. An energetic polymer can be added between the substrate and the absorber. With 10 μ s duration near-IR exposure pulses, the energetic layer has no discernable effect. With 110 ns imaging pulses, exposed spots in imaging media with energetic underlayers can be more than three times larger. The improvement due to energetic polymers results from confining the hot gas-phase thermochemical decomposition products under the silicone layer, as shown by time-resolved microscopy. The force exerted by the expanding bubble tears the neck of the bubble away from the substrate, increasing the imaged spot size. These rather complicated processes cannot be described by previously used simple exposure threshold models. An exposure parameter is introduced which deals with this problem. In some cases energetic material underlayers can improve the sensitivity of the media by a factor of three. This work is believed to be the first where a substantial sensitivity improvement in laser threshold for photothermal imaging is obtained with energetic polymers.

Journal of Imaging Science and Technology 44: 111–119 (2000)

Introduction

Laser photothermal materials are widely used in imaging applications including printing, proofing, computer-to-plate, and computer-to-press.^{1,2} These materials, typically exposed by pulses of near-infrared (near-IR) light from inexpensive solid-state lasers, show an inherently nonlinear response to light since there is a relatively sharp imaging fluence threshold for short duration laser pulses, but essentially no response to ambient light.^{1–5} Understanding the fundamental mechanisms of laser photothermal imaging is complicated because the materials themselves are usually complicated multilayer formulations, and their practical applications combine the disciplines of imaging science, optical physics, mechanical engineering, solid-state physics and solid-state thermochemistry.

One challenge in the field is to reduce the imaging threshold fluence while maintaining desirable properties such as durability, manufacturability, compatibility with other imaging materials and so on. This challenge is motivated by the relatively high cost of laser photons, compared to the imaging materials themselves. One intriguing strategy for reducing the imaging threshold involves energetic materials. The idea is to use some of the chemical energy in the material to assist the laser in the imaging process.⁶

Almost since the development of the laser, there have been sporadic attempts to realize this strategy by in-

corporating energetic polymers such as NC^{7,8} (nitrocellulose), acrylic polymers,⁹ GAP (glycidyl azide polymer), BAMO (bis(azidomethyl)oxetane polymer), and AMMO (azidomethyl methyloxetane polymer)^{6,10} into various photothermal imaging materials used for laser material transfer.³ The latter three polymers can be used as propellants, and they generate N₂ gas upon heating, which was hoped to assist laser material transfer.^{6,10} This effort and the history of this approach was recently reviewed.^{6,10} Although it was initially believed that self-oxidizing binders such as NC were needed for good photothermal ablation, as in laser ablation transfer imaging,^{7,8,11} it was subsequently shown that self-oxidizing binders were not needed.¹² Even imaging materials with explosive layers (as opposed to self-oxidizing layers) such as GAP, BAMO and AMMO did not have lower exposure thresholds than other common photothermal materials used in similar applications. Subsequent work on energy release by laser heating and by shock detonation of GAP suggested that chemical reactivity of GAP might be too slow to be of much use in photothermal imaging.^{6,13,14}

In the present work, we investigate the effects of adding a thin layer of energetic polymer to a model photothermal imaging material. We show that under some circumstances the energetic polymer can greatly increase the sensitivity to laser light. The result is particularly interesting, beyond even the practical implications, because it provides insights into ways of understanding and optimizing these complicated systems, and it causes us to rethink the widely used concept of “threshold fluence”.

The imaging materials used here are model systems based on the PEARLTM system developed by Presstek, Inc. (Nashua, NH) for computer-to-press and computer-to-plate imaging.^{15,16} As depicted in Fig. 1, a system we

Original manuscript received June 2, 1999

▲ IS&T Member

To whom correspondence should be addressed; dlott@scs.uiuc.edu

©2000, IS&T—The Society for Imaging Science and Technology

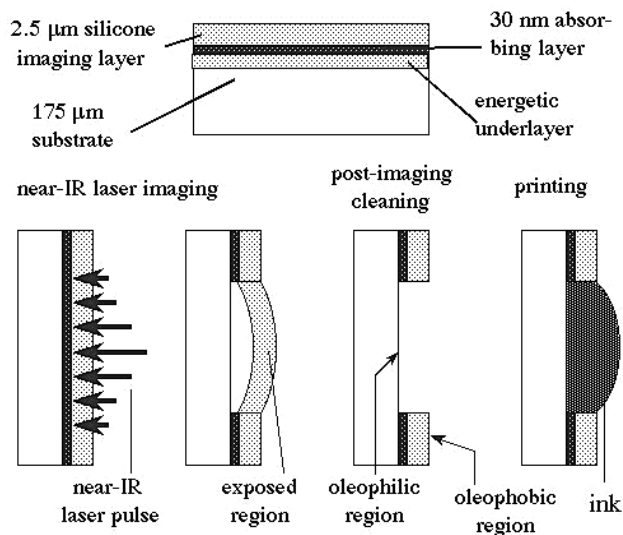


Figure 1. Schematic of the imaging medium. After exposure by a near-IR pulse, the silicone imaging layer is released. After post-imaging cleaning, the exposed region has an affinity for ink. The basic imaging medium has no underlayer. An acrylic or nitrocellulose energetic underlayer is added to some samples.

will term the “basic imaging medium” consists of a polymer substrate, a nanometer thick absorbing layer, and a micrometer thick surface imaging layer which is oleophobic (ink hating). A near-IR laser pulse incident on the material causes rapid heating of the absorbing layer. The substrate is thermochemically inert compared to the imaging layer. Gas-phase thermal decomposition products are generated at the interface of the absorbing layer and the imaging layer, which are trapped under the tough silicone imaging layer. A bubble is formed in the imaging layer. The neck or base of the bubble is in the plane of the substrate. Bubble formation permanently reduces the adhesion of the imaging layer.^{15,16} The region of the imaging layer exposed by the laser pulse can be removed by post-exposure cleaning to produce an oleophilic (ink loving) spot. An image is produced as a series of spots, by an imaging engine which scans and modulates the laser.¹⁵ The exposed material can be used as a plate for extended runs (~300,000) on an offset dry lithographic printing press.^{15,16} For the purposes of this study, modifications have been made to the basic imaging medium by adding energetic polymer underlayers, as shown in Fig. 1.

In previous works,^{16–19} we used pulse-width dependent time-resolved optical microscopy to show that the basic imaging medium has a well-defined laser fluence threshold which is independent of laser spot size for spots bigger than¹⁹ 10 μm. The medium is not imaged properly for pulse durations greater than¹⁹ ~30 μs. With shorter duration pulses, the threshold decreases with decreasing pulse duration.¹⁹ The pulse duration dependence in the 1 ps – 30 μs range was explained by a thermal conduction model which postulated that imaging occurred when the interface attained a threshold temperature¹⁹ T_{th} . (Data from the thermal conduction model yielded a value $T_{th} = 550^{\circ}\text{C}$.) Time-resolved microscopy was used to examine the roles of the different layers in the imaging process.¹⁷ In the present work, the properties of new media are studied, where an additional energetic underlayer can be added between the absorbing layer and the substrate.

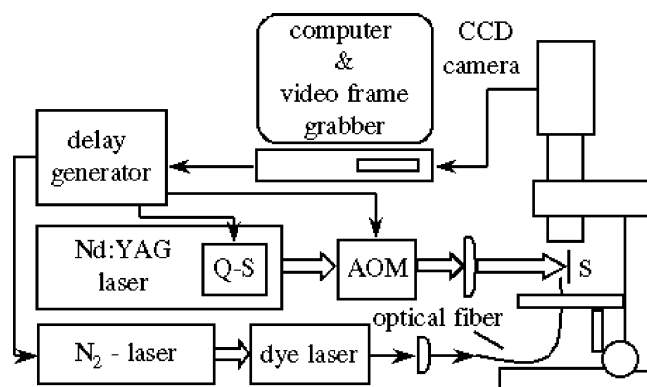


Figure 2. Block diagram of experimental apparatus. The side-view imaging configuration is shown. AOM = acousto-optic modulator, Q – S = Q-switch. S is the imaging sample.

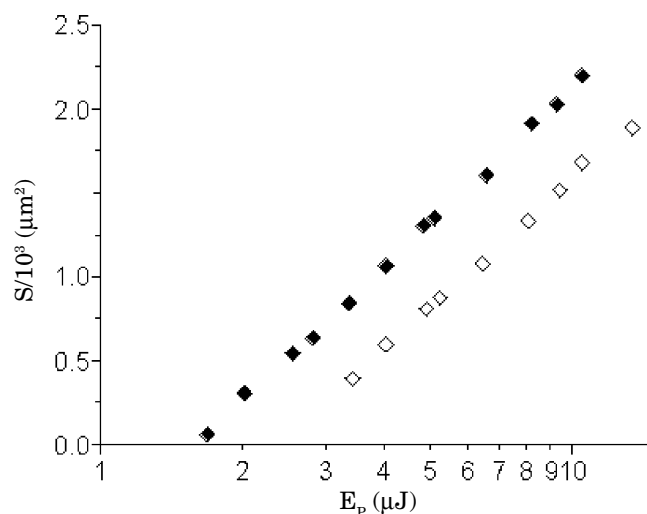


Figure 3. Area S of exposed spot with 10 μs laser pulses, as a function of pulse energy E_p , for the basic imaging medium. The laser beam radius is $r_0 = 28$ μm. Filled symbols denote substrate with bare Ti absorber. Open symbols denote substrate with absorbing layer and silicone imaging layer, with cleaning.

Experimental

Materials. A series of three pairs of different imaging media were studied. Each pair consisted of a substrate with just the bare absorbing layer, and a substrate with the absorbing layer covered with an additional polydimethyl siloxane (silicone) imaging layer. The substrates were 175 μm thick DuPont polyester films, either Melinex™ 329 or Melinex™ 339 (DuPont Corp., Wilmington, DE). Melinex films are glossy white polyester with a micrometer-scale surface granularity (e.g. see Fig. 4). The absorbing layer was coated on the substrate by sputtering ~30 nm of titanium.^{15,16} This thin metallic layer, which undoubtedly contains oxides as well as metallic Ti, was tailored to maximize near-IR absorption. The Ti layer absorbs ~50% of incident light and transmits ~20%.¹⁶ The white polyester substrates were used to decrease the threshold fluence by reflecting most of the transmitted light back into the absorbing layer. The silicone rubber imaging layer was applied at a density of 2.5 g/m², which produces a coating ~2.5 μm thick.

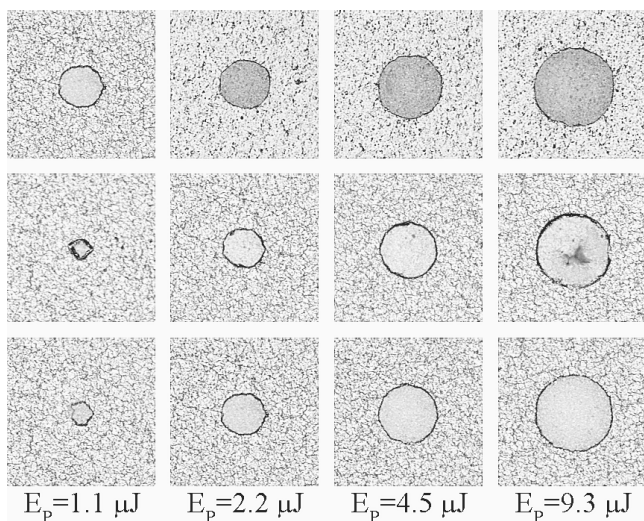


Figure 4. Spots exposed in the basic imaging medium by 110 ns 28 μm radius laser pulses. E_p denotes pulse energy. Images are $135 \times 135 \mu\text{m}^2$. Top row: substrate with bare Ti absorber. Middle and bottom rows: substrate with absorber and silicone imaging layer. Middle row: exposed medium prior to cleaning. Bottom row: same spots as middle row with post-imaging cleaning.

When the media were imaged by laser pulses, three different states could be produced. In media with bare metallic absorbing layers, an imaged area could be produced where the metal thin film was removed. In media with an additional silicone imaging layer, an area could be produced where the silicone bubbled up, and the underlying metal thin was removed. When these media were subjected to a post-imaging cleaning process (Fig. 1), the silicone imaging layer in the vicinity of the exposed spot could be removed. The silicone coated materials were cleaned by gentle rubbing with a soft cotton pad moistened with isopropyl alcohol. The diameter of the cleaned spot was not really dependent on how the material was cleaned, although some coatings could be torn if rubbed very hard.

Two pairs of imaging media were fabricated to investigate the effects of energetic polymer underlayers (Fig. 1). One pair, with an energetic acrylic underlayer, was fabricated on a Melinex™ 339 substrate, which differs from the 229 substrates by an additional surface layer, a very thin (perhaps $\sim 0.1 \mu\text{m}$) acrylic polymer coating. Acrylic polymers decompose with moderate exothermicity and can explode when heated rapidly, in part because of a favorable oxygen balance due to the ester groups.²⁰ A second pair with an energetic NC underlayer was also fabricated on a Melinex™ 339 substrate, by coating an additional $\sim 1 \mu\text{m}$ thick layer of highly cross-linked, highly nitrated NC ($\sim 11\%$ N by weight, compared to a theoretical maximum of $\sim 13\%$ by weight²¹). NC, also known as “gun cotton” decomposes with moderately high exothermicity, due to the presence of NO_2 groups which provide excellent oxygen balance, and it can explode violently when rapidly heated.

Threshold Measurements

As shown in Fig. 2, imaging materials were exposed with near-IR pulses from a continuously-pumped Nd:YAG (YAG denotes yttrium aluminum garnet) laser at $1.064 \mu\text{m}$ wavelength.^{17,19} To produce nearly rectangular $10 \mu\text{s}$ pulses, the continuous output of the laser was chopped with an external acousto-optic modulator.

When the laser was Q-switched, it produced a pulse whose FWHM is 110 ns. The laser pulse spatial profile is close to a TEM_{00} Gaussian beam with a slight ellipticity, which was verified using a beam profile analyzer (Spiricon). The beam radius r_0 is about $28 \mu\text{m}$ at the focal plane, although there was a slight variation of the radius, with the exact value depending on daily variations of the thermal load on the Nd:YAG laser crystal.

For threshold measurements, the sample was placed on the microscope stage with the silicone coating facing up. A calibrated photodiode was used to measure laser pulse energy E_p . A thin pellicle dichroic beamsplitter was placed at 45 degrees between the objective and the material, which reflects the near-IR pulse onto the sample, while allowing the sample to be viewed by transmitting visible illumination from the microscope’s tungsten lamp. Placing the sample on the microscope stage allows focusing the laser beam on the material with great precision. The exposed samples were cleaned and re-placed on the microscope stage. Images were obtained with a video camera and video frame grabber. Image analysis software (Data Translation Global Lab Image™) was used to determine the exposed area.¹⁷

Consider a laser beam with a Gaussian spatial profile with Gaussian beam radius r_0 . The fluence $J(r)$ decreases moving radially outward from the beam center. A spatially averaged fluence is usually defined as $J_{\text{avg}} = E_p/(\pi r_0^2)$, where E_p is the laser pulse energy. $J(r)$ is given by,^{4,16,22}

$$J(r) = 2J_{\text{avg}} \exp\left(-\frac{2r^2}{r_0^2}\right), \quad (1)$$

where $J(0) = 2J_{\text{avg}}$. It is usually assumed there exists a sharp threshold fluence J_{th} for a particular pulse duration, which is independent of r_0 . When the fluence incident at any location of the material exceeds the threshold fluence, that location becomes exposed,^{4,16,22} independent of what happens at any other location. In this case, which we might term the “local threshold model”, the exposed spot area S is a circular region with spot radius r_s , which depends on the fluence,^{4,16,22}

$$S = \pi r_s^2 = 0 \quad J(0) < J_{\text{th}} \\ S = \pi r_s^2 = \frac{\pi r_0^2}{2} \ln\left(\frac{2E_p}{J_{\text{th}}\pi r_0^2}\right) \quad J(0) \geq J_{\text{th}}. \quad (2)$$

Equation 2 shows the exposed spot radius increases with increasing fluence J above the threshold fluence J_{th} . It has also been shown that the radius of the exposed spot grows with time during the laser pulse.²² Equation 2 shows that a plot of the exposed area S versus the logarithm of the laser pulse energy E_p should be linear. The slope of the line should be proportional to r_0^2 , and the line should cross the abscissa at $E_p = 2J_{\text{th}}\pi r_0^2$. Notice that Eq. 2 describes a *local exposure model*, where the behavior of any location in the imaging medium is *independent of what happens at other locations*.

For materials which obey Eq. 2, there is a point of maximum efficiency, where the amount of wasted laser energy is a minimum.^{4,18} When the fluence is below J_{th} , the exposed area $S = 0$ and all the energy is wasted. Due to the logarithmic dependence in Eq. 2, fluences much greater than J_{th} do not increase the exposed area much.⁴ The point of maximum efficiency occurs when $r_s^2 = (2)^{-1/2}r_0^2$ and the exposure fluence is $J = J_{\text{th}}\exp(1) \approx$

$2.7 J_{th}$. It will be useful to work with exposed areas. Defining an effective area for the laser beam, $S_0 = \pi r_0^2$, the point of maximum efficiency occurs when $S = S_0/2$. In our experiments, $r_0 = 28 \mu\text{m}$, so $S_0 = 2.5 \times 10^3 \mu\text{m}^2$.

Time-Resolved Microscopy

The time-resolved microscopy apparatus has been described previously.¹⁶ A new feature has been added, which lets us obtain a side-view of the imaging material.¹⁷ Essentially a shadowgraphy technique, the layout for side-view imaging is shown in Fig. 2. The imaging material is placed in a holder facing the imaging pulses, with a few degree tilt. The microscope is carefully focused onto the spot in the medium where the imaging pulse hits. Each time the imaging laser is fired, a single image is obtained by illuminating the sample with a sub-nanosecond probe pulse from a N_2 -laser pumped dye laser. To reconstruct the time-dependent imaging process, a series of images is obtained at different times, each image from a fresh spot on the sample. The exposure process is reproducible enough that this series of images accurately represents the actual time-dependent exposure process.¹⁶

Results

Exposure with 10 μs pulses

When substrates with only the bare Ti coating were imaged with 10 μs pulses, the metallic layer was removed from the imaged area. The mechanism involves melting and receding of the melt layer due to surface tension of the liquid metal.¹⁷ This type of imaging process, involving thin metal films on a polymer support imaged by longer duration pulses, has been studied a great deal, as it is the basis of the compact disk (CD) industry. The behavior of the basic imaging medium (substrate, Ti absorbing layer, 2.5 μm silicone imaging layer) imaged by 10 μs pulses, has been discussed in previous publications.^{16,17} During the laser pulse, the silicone layer formed a bubble that puffed up from the surface, as diagrammed in Fig. 1. When the silicone layer was cleaned, round exposed spots were formed with smooth, sharply defined boundaries. Some typical threshold data are shown for the basic imaging media in Fig. 3. The data for the medium with a silicone imaging layer refer to the exposed spot size after cleaning. The linear behavior predicted by Eq. 2 is observed with 10 μs pulses for all six materials, over a fluence range between J_{th} and about 5-10 times J_{th} . The slope of the data gives the expected beam radius $r_0 = 28 \mu\text{m}$. The threshold fluences for the basic imaging media were $136 \pm 5 \text{ mJ/cm}^2$ (bare metallic absorber) and $215 \pm 3 \text{ mJ/cm}^2$ (with silicone imaging layer). Adding the silicone imaging layer increases the fluence, since it increases the conduction of heat away from the absorbing layer.¹⁹ The error bounds, indicating one standard deviation, are determined by standard linear regression analysis. The exposure fluence thresholds for all six imaging materials are given in Table I. The energetic underlayers did not noticeably decrease the exposure threshold with 10 μs pulses.

Exposure with 110 ns pulses

In previous works from our laboratory, time-resolved microscopy was used to document the differences between the 10 μs and 110 ns exposure process of the basic imaging medium.^{17,19} At 10 μs the Ti melts; at 110 ns it boils off the substrate.¹⁷ At 10 μs , the silicone coating puffs up slightly from the substrate; at 110 ns, it blows up into a rapidly expanding bubble.¹⁷ However the end

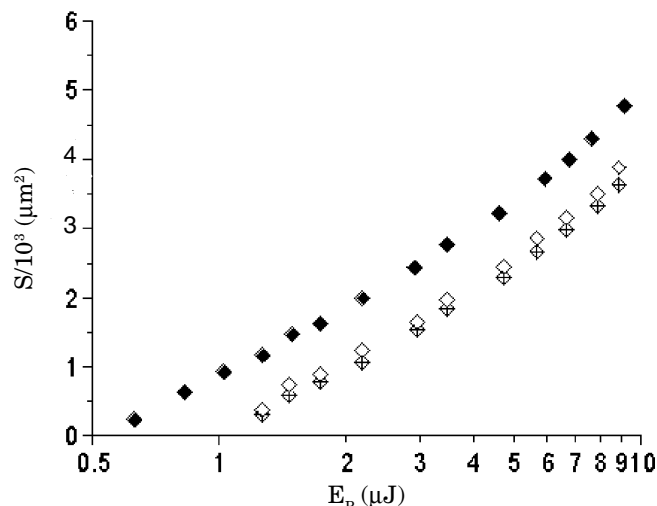


Figure 5. Area S of exposed spots in basic imaging media as a function of pulse energy E_p , with 110 ns, 28 μm radius laser pulses as in Fig. 4. Solid symbols: substrate with bare Ti absorber. Open symbols: exposed region with silicone imaging layer. Crossed symbols: same as open symbols, but with post-imaging cleaning.

result is practically the same, and the exposed spot with post-imaging cleaning is practically indistinguishable with the two pulse durations.¹⁹

The most interesting result of this study is that *entirely new phenomena emerge with 110 ns pulses in materials with energetic underlayers*. We begin by showing results at 110 ns for the basic imaging medium with no energetic layer (Figs. 4 and 5). Figure 4 shows three rows of spots exposed at different fluences, viewed in a reflection-illumination geometry. The top row shows the imaged medium with bare Ti. The middle row shows imaged spots in the medium with a silicone layer. The bottom row shows imaged spots from the middle row after cleaning, which reveals a nicely round spot with smooth edges, with about the same area as the region where Ti was removed. Figure 5 is a plot of imaged area S versus pulse energy. The three symbols in Fig. 5 correspond to the three rows of Fig. 4. They indicate imaged area with bare Ti, imaged area with the silicone coating, and imaged area after cleaning the silicone layer. The imaged spot areas increase linearly with pulse energy E_p , from threshold fluence to about ten times threshold. Since the threshold is lower with 110 ns pulses and more laser power can be obtained in the Q-switching mode, we can continue the plot to higher multiples of the threshold fluence than was possible with 10 μs pulses (Fig. 3). A deviation from linearity (an increase in slope) is seen at the higher fluences. The deviation is of the form that at the higher fluences, *more area* is exposed per unit energy than was expected. The slopes obtained from these data in the lower energy regime give the expected laser beam radius of $r_0 = 28 \mu\text{m}$. The thresholds obtained by fitting the data at lower energies were $36.4 \pm 0.7 \text{ mJ/cm}^2$ (bare metallic absorber) and $60.2 \pm 4.7 \text{ mJ/cm}^2$ (with silicone imaging layer).

Data for media with the acrylic underlayer are shown in Figs. 6 and 7. The acrylic underlayer data are practically the same as the basic imaging medium (Fig. 3) with one important difference. The imaged area grows noticeably larger after cleaning. The cleaned spots in this case (Fig. 6) sometimes show a perimeter which is a bit more ragged than in the basic imaging medium (Fig. 4).

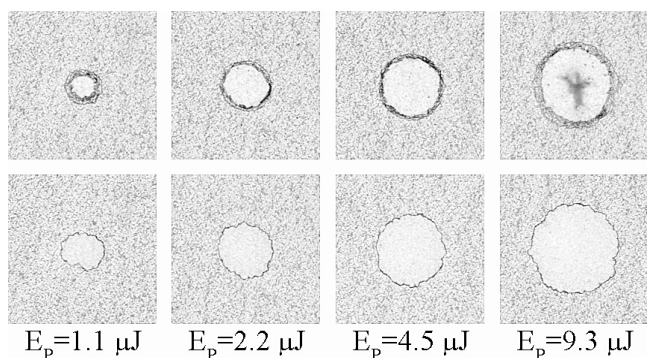


Figure 6. Spots exposed by 110 ns, 28 μm radius pulses in imaging medium with acrylic underlayer and silicone imaging layer. Image size is $135 \times 135 \mu\text{m}^2$. Top row: before cleaning. Bottom row: with post-imaging cleaning. After cleaning, the imaged area increases somewhat.

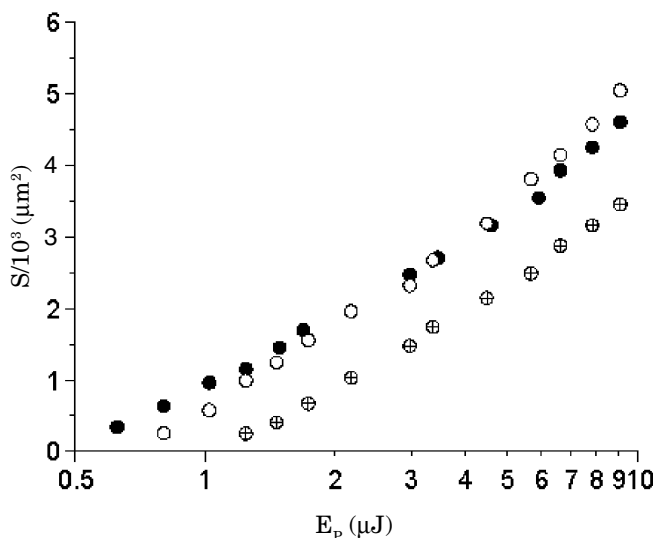


Figure 7. Area S of exposed spots in imaging media with energetic acrylic underlayer as a function of pulse energy E_p , with 110 ns, 28 μm radius laser pulses as in Fig. 6. Solid symbols: substrate with bare Ti absorber. Crossed symbols: exposed region with silicone imaging layer. Open symbols: same as crossed symbols, but with post-imaging cleaning. The imaged area increases somewhat with cleaning, especially at larger pulse energies.

Because the cleaned spots with the acrylic underlayer are considerably larger than without this underlayer (Fig. 7), in some sense (*vide infra*) the underlayer has increased the sensitivity of this imaging medium to laser light.

Data with the NC underlayer are shown in Figs. 8 and 9. The data in Fig. 9 are similar to what is seen in Figs. 5 and 7 except that once the silicone imaging layer is cleaned, the exposed area increases dramatically, by up to a factor of five. The large increase in area is evidently related to the new feature seen in Fig. 8. Prior to cleaning, the exposed spot appears as a circular zone comparable in size to that seen in the other materials, but in addition it is surrounded by an annular zone of collateral damage in the silicone coating, which can be removed by post-imaging cleaning. The data in Fig. 9 for the cleaned material with NC shows a strong deviation from the linear behavior predicted by Eq. 2, so the simple threshold model cannot be used here.

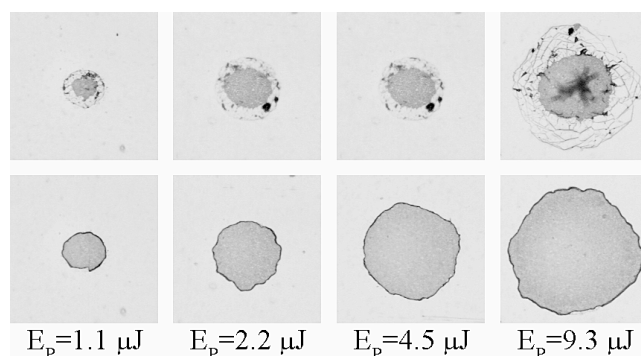


Figure 8. Spots exposed by 110 ns, 28 μm radius pulses in imaging medium with nitrocellulose (NC) underlayer and silicone imaging layer. Image size is $135 \times 135 \mu\text{m}^2$. Top row: before cleaning. The darker region in the center indicates Ti was removed. The outer annular region is formed when the silicone layer is torn away from the substrate. Bottom row: After post-imaging cleaning, the imaged area becomes up to four times larger.

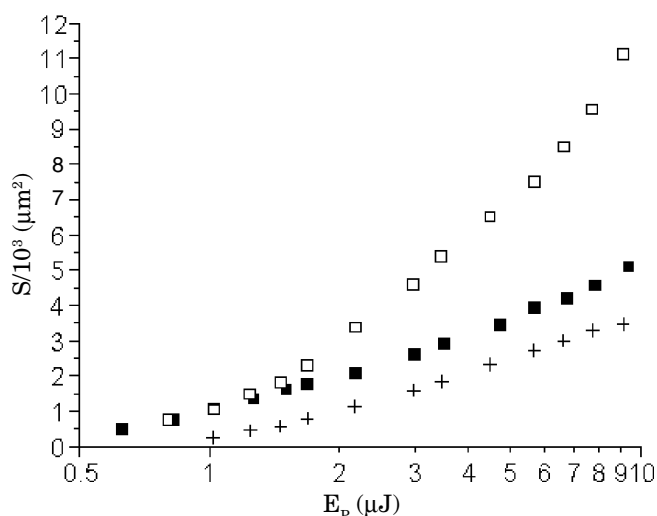


Figure 9. Area S of exposed spots in imaging media with energetic nitrocellulose (NC) underlayer as a function of pulse energy E_p , with 110 ns, 28 μm radius laser pulses as in Fig. 8. Solid symbols: substrate with bare Ti absorber. Crossed symbols: exposed region with silicone imaging layer. Open symbols: same as crossed symbols, but with post-imaging cleaning. The imaged area increases dramatically with cleaning, especially at larger pulse energies.

Time-Resolved Microscopy

To better understand the effects of the NC underlayer, we compared the basic imaging medium to the NC medium with time-resolved side-view microscopy. The pulse energy in both cases was 12 μJ , which is at the highest end of the range plotted in Figs. 5 and 9. The NC has the greatest effect at the largest pulse energies. Figure 10 shows the results in the basic imaging medium without NC. Hot gas-phase thermal decomposition products formed at the Ti:silicone interface cause the silicone layer to blow off the substrate at a velocity of about 100 m/s. The silicone is very tough, so the hot gas is confined in a silicone bubble. The neck of the bubble (in the plane of the imaging medium) is the darkened region at the left of each image panel. During the laser pulse (e.g.

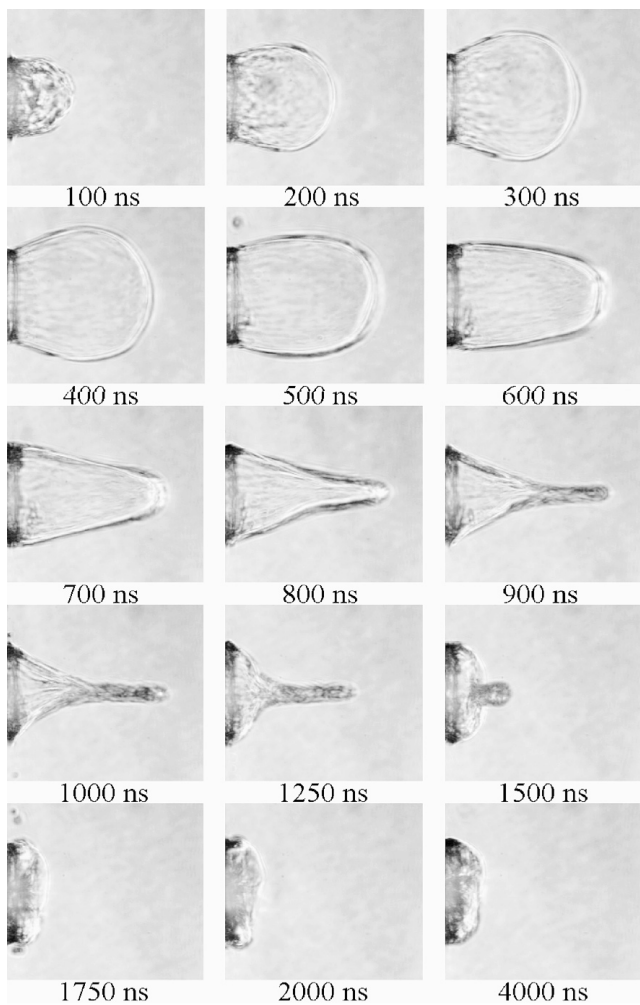


Figure 10. Side-view images of the basic imaging medium, consisting of substrate, Ti absorbing layer, and silicone imaging layer, exposed by 12 μJ , 110 ns, 28 μm diameter pulses. Image sizes: 135 \times 148 μm^2 . A bubble is formed in the tough silicone coating. The dark region to the left of each image is the neck of the bubble in the plane of the imaging medium.

in the 0-200 ns time range) the diameter of the neck increases with time. The neck diameter at the end of the pulse approximately corresponds to the diameter of the cleaned exposed region in the medium. The bubble continues to expand for a few hundred ns. Eventually cooling caused by the rapid expansion and by thermal conduction into the substrate causes the bubble to stop expanding and begin contracting. The bubble then snaps back, hitting the substrate, bouncing a few times and eventually settling down.¹⁷

Figure 11 shows the same sequence with the NC underlayer. Everything is about the same as in Fig. 10 for the first 300 ns or so, but then the bubble continues to grow. Image analysis software was used to measure the cross-sectional area of the bubbles in Figs. 10 and 11 as a function of time, as shown in Fig. 12. With NC, the cross-sectional area at its maximum is more than twice as large as without NC, which implies the maximum volume and the amount of hot gas generated is perhaps three times as great with NC, based on volume = area^{3/2}. The additional bubble growth has a profound effect on the neck region. At about 300 ns, a more prominent neck region develops at the left of each panel. In

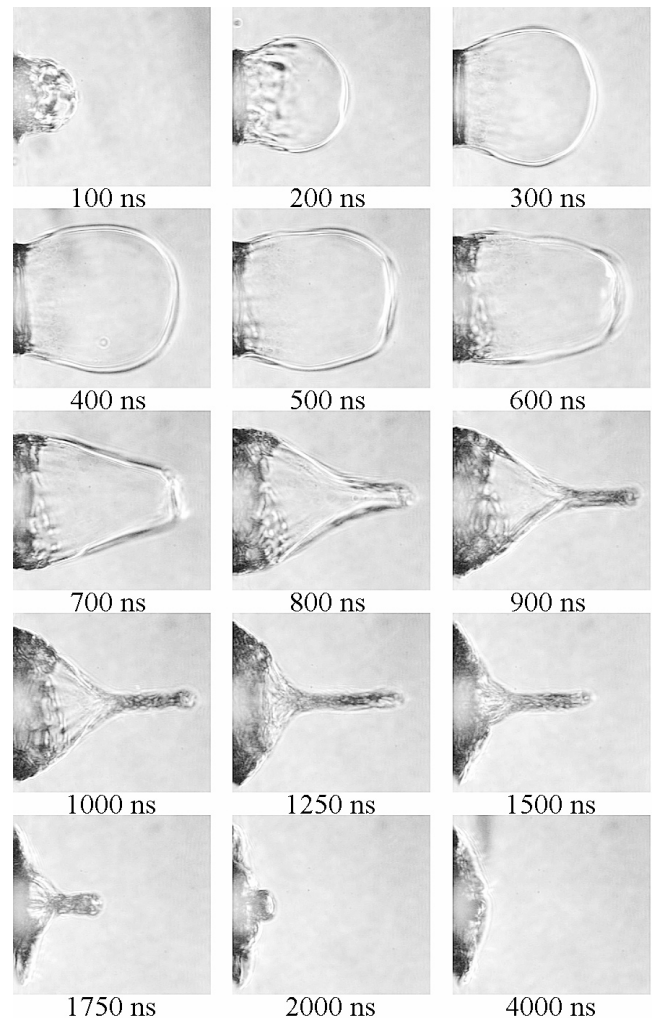


Figure 11. Side-view images of imaging material as in Fig. 10, but with nitrocellulose (NC) underlayer. Image sizes: 135 \times 148 μm^2 . With NC, the bubble size after 300 ns is greater than in Fig. 10. As the bubble grows larger, the neck of the bubble in the plane of the imaging medium (far left) suddenly enlarges.

the 600-1200 ns range, the bubble neck enlarges substantially, so at the end of the image sequence, the neck is noticeably larger with NC (Fig. 10).

Discussion

With the energetic NC underlayer, more hot gas is generated, which stretches the bubble further. In Fig. 11, the volume of hot gas is up to three times as great as without NC. That alone would not increase the imaged spot radius, but a second process occurs. After about 300 ns, the neck of the bubble begins to expand substantially. The sudden expansion of the neck is attributed to the force exerted by the edges of the bubble on the imaging layer. When this force exceeds the adhesion of the imaging layer to the substrate, the imaging layer tears away from the substrate. In this case the central spots in Fig. 8 would indicate regions where Ti is removed by the laser pulse, and the annular region would indicate regions of the silicone imaging layer which have been torn away from the substrate. This tearing process is depicted schematically in Fig. 13. The slightly greater diameter of cleaned imaged spots in

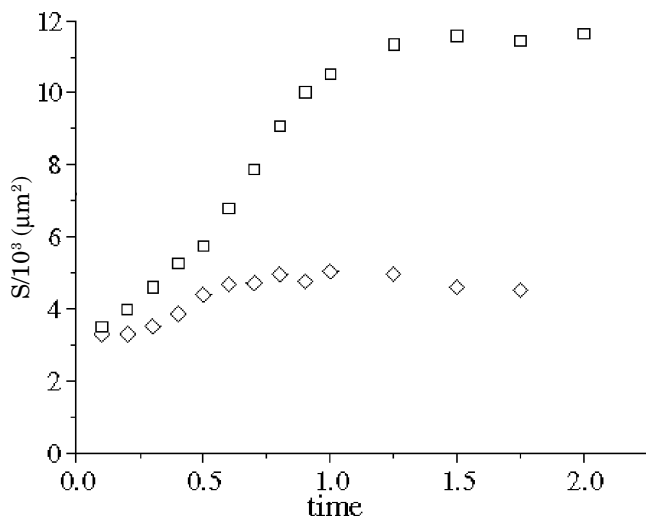


Figure 12. Time-dependent areas of bubbles in Figs. 10 and 11. Open diamonds: no energetic underlayer. Open squares: with nitrocellulose (NC) underlayer.

material with an acrylic underlayer is also attributed to this tearing process. With the acrylic layer, it is not certain that more gas is formed during exposure, so it is possible the tearing process might occur simply because the acrylic layer reduces the adhesion of the imaging layer to the substrate.

The tearing process is clearly an example of *non-local behavior*. Generally speaking, non-local behavior means that excess energy above threshold deposited at one region can be transmitted to other nearby regions. The result is an imaged spot that is larger than would be expected in the case of strictly local behavior, i.e. an increase in slope at higher intensities in plots such as Figs. 5, 7 and 9. With a Gaussian beam profile, there is always excess energy at the center of the beam above threshold. For example, at the point of maximum efficiency, the intensity at the center is $\exp(1)$ times threshold. In the present case, energy deposited at the center of the irradiated spot is transmitted to the perimeter of the irradiated spot, where it is used to increase the spot radius, by the rapid expansion of the tough silicone bubble. In analogy to a well-known property of explosives, the effects of energetic materials may be amplified by confining the blast, in this case within the silicone bubble. Confining the explosion seems to be an important concept which should be considered in future designs of photothermal materials with energetic layers.

Because the threshold model of Eq. 2 describes only local exposure phenomena, we need a new way of quantifying the behavior of the imaging media with energetic material layers. Earlier, we defined a parameter $S_0 = \pi r_0^2$, where r_0 is the Gaussian beam radius, which represents the effective area of the laser beam. Materials which obey Eq. 2 are ordinarily operated near the point of maximum efficiency,^{4,18} where the exposed area is $S_0/2$. Because the intensity of a Gaussian profile pulse falls off rapidly beyond r_0 , it takes a substantial excess of laser energy to expose a spot much larger than S_0 . For example, to expose a spot whose area is S_0 , the incident fluence $J \approx 7.4 J_{th}$ (i.e. $\exp(2)$ times J_{th}), and to produce a spot whose area is $4S_0$, $J \approx 3000 J_{th}$ (i.e. $\exp(8)$ times J_{th}).

To motivate this discussion, let us consider results for a relatively large pulse energy $E_p = 10 \mu J$, where the

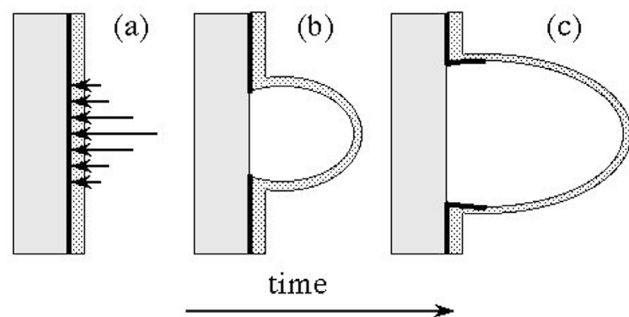


Figure 13. Schematic depiction of the exposure process with 110 ns pulses. (a) Imaging medium is irradiated by a pulse with a Gaussian profile. (b) Rapid expansion of a bubble in the silicone imaging layer is caused by generation of hot gas-phase thermal decomposition products. (c) With NC underlayer, more gas is generated. The additional force tears the imaging layer from the substrate, enlarging the imaged region.

effects of energetic underlayers are great. For our experiments, $S_0 = 2.5 \times 10^3 \mu m^2$. With 10 μs duration pulses at this pulse energy, the exposed areas for all the materials studied were $S \approx 1.7 \times 10^3 \mu m^2$ (e.g. Fig. 3). With 110 ns duration pulses, the exposed areas in all the imaging media are larger because the threshold decreases with decreasing pulse duration¹⁹ (non-reciprocal behavior). With 110 ns pulses and the basic imaging medium with no energetic layer, the imaged area is a bit more than twice as large, $S \approx 3.6 \times 10^3 \mu m^2$ (see Fig. 5). With the acrylic underlayer, $S \approx 5.5 \times 10^3 \mu m^2$ (Fig. 7), so adding the acrylic underlayer produces an exposed spot about 50% larger. With the NC underlayer, $S \approx 12 \times 10^3 \mu m^2$ (Fig. 9), so adding the NC underlayer produces an exposed spot about 3.3 times larger. In this example with NC, the exposed area $S \approx 4S_0$, which as shown above ordinarily requires a fluence $J \approx 3000 J_{th}$. Thus the effects of the NC layer are, without fear of overstatement, little short of astounding.

We now introduce an exposure parameter Σ , which characterizes the sensitivity of the imaging material to light. Σ is a measure of how much laser energy is needed to expose a region of area S ,

$$\Sigma = E_p/S. \quad (3)$$

It is evident that Σ may be a function of pulse duration, fluence, imaging material properties, and possibly the imaged spot size. Σ is useful, in that it tells how much energy is needed to expose an imaging material of a given area. It is desirable to minimize Σ , since materials with smaller values of Σ are more sensitive to laser light.

For materials which obey Eq. 2, the exposure parameter behaves as follows. $\Sigma = \infty$ for pulse fluences below threshold, because the exposed area $S = 0$. Σ is a minimum at the point of maximum efficiency, where $\Sigma = J_{th} \exp(1) \approx 2.7 J_{th}$. Then Σ increases gradually with fluence, for fluences above the point of maximum efficiency. Figure 14 is a plot of Σ versus fluence J for 110 ns pulses ($r_0 = 28 \mu m$), for imaging media with and without energetic layers. From this plot, the minimum values of the exposure parameter can be determined. The minimum for the basic imaging medium occurs near the point of maximum efficiency, since this medium obeys the local threshold model reasonably well.

The values of the exposure parameter Σ for 10 μs and 110 ns pulses are given in Table I. For materials which

TABLE I. Threshold Fluences and Exposure Parameters for Imaging Media

Underlayer	Silicone imaging layer	Exposure fluence J (mJ/cm ²) for 10 μ s pulses	Exposure parameter Σ (mJ/cm ²) for 10 μ s pulses	Exposure parameter* Σ (mJ/cm ²) for 110 ns pulses
none	no	136 \pm 5	368 \pm 14	99 \pm 2
none	yes	215 \pm 3	583 \pm 8	178 \pm 6
acrylic	no	152 \pm 4	412 \pm 11	98 \pm 5
acrylic	yes	190 \pm 15	515 \pm 41	111 \pm 8
nitrocellulose	no	139 \pm 6	377 \pm 16	87 \pm 5
nitrocellulose	yes	204 \pm 16	553 \pm 43	55 \pm 4

*The value cited is the maximum sensitivity (minimum value of Σ)

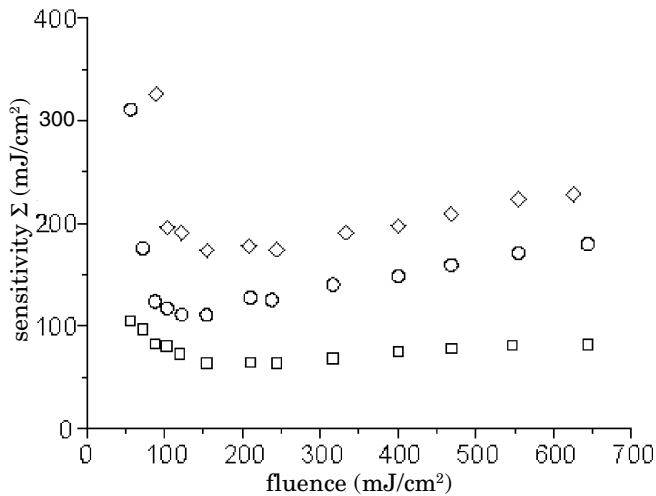


Figure 14. Plot of exposure parameter $\Sigma = E_p/S$, where S is the exposed area, versus pulse fluence J for imaging materials with no underlayer (diamonds), with acrylic underlayer (circles) and with NC underlayer (squares). Smaller values of Σ indicate greater sensitivity. Media with the NC underlayer can be three times more sensitive than media with no underlayer.


fit the threshold model, Σ is computed using $\Sigma = J_{th} \exp(1)$. For other materials, the table lists the minimum value of Σ . With no energetic layer, the minimum value is $\Sigma \approx 180$ mJ/cm². With the acrylic layer, the minimum value is $\Sigma \approx 110$ mJ/cm². With the NC layer, the minimum value is $\Sigma \approx 55$ mJ/cm². Thus the NC underlayer provides an increase in sensitivity of a factor of more than three over the basic imaging medium.

Summary and Conclusions

Prior to the present work, efforts to substantially lower the fluence threshold of laser photothermal imaging materials by incorporating energetic materials were largely unsuccessful.^{6,10} In the present work, a photothermal imaging medium which can be used as a printing plate in computer-to-plate or computer-to-press applications, was modified by incorporating an energetic polymer, either acrylic polymer or nitrocellulose (NC), in an underlayer between the absorbing layer and the substrate. With 10 μ s duration laser pulses, the energetic materials had essentially no effect on the imaging threshold fluence J_{th} . With 110 ns duration laser pulses, dramatic effects were observed with the NC underlayer, and to a lesser extent with an acrylic underlayer. Although the widely used threshold model of Eq. 2 sufficed to describe the exposure process at 10 μ s, and even at 110 ns in the basic imaging medium (and in many

other photothermal materials), it failed for materials with energetic layers and 110 ns pulses. The failure of this simple model was attributed to nonlocal effects, namely that energy absorbed at the center of the imaged spot could be transmitted to the perimeter of the imaged spot, to enlarge the imaged region. The mechanism of nonlocal effects was shown by time-resolved side-image microscopy, to involve the formation of a bubble in the tough silicone imaging layer, which exerted large transient forces at its neck. The transients tear the imaging layer away from the substrate, enlarging the imaged region. In other words, the effects of the energetic underlayers were enhanced by confining the hot gas-phase thermal decomposition products under the silicone bubble. The composition of the energetic underlayer may also affect the adhesion of the imaging layer to the substrate. The tearing effect is enhanced by generating more gas, and by reducing the adhesion. However if the adhesion is lowered too much, the imaging medium loses its durability. With 10 μ s pulses, the bubble expansion was too gradual to enlarge the exposed region. With 110 ns pulses the bubble expands more forcefully, but not enough to enlarge the exposed region in the basic imaging medium (Fig. 10). Adding a NC energetic underlayer causes the bubble to expand to about three times greater volume, which produced enough force to enlarge the imaged region. The expansion of the imaged region is related to the greater volume of gas produced, and it may also be a reflection of a difference in adhesion between the substrate and imaging layer caused by introducing the energetic layer.

The economic consequences of lowering the threshold fluence of laser photothermal imaging materials can be substantial. Although the energetic material systems studied here do not obey a simple threshold model, it was possible to define an exposure parameter Σ to characterize these materials. Adding an NC underlayer improved the sensitivity by a factor of three. Even a 15% improvement, such as that obtained by substituting a reflective white substrate for a transparent substrate, is regarded as significant for practical applications, so this is a remarkable result. The sensitivity improvement from energetic underlayers involves producing an exposed area which is considerably larger than the effective area of the laser pulse S_0 . That should not be taken to imply that such materials must be used only in low-resolution applications, since one could design imaging engines to focus the laser beam somewhat tighter than the desired size of the imaged spots. In fact, commercial imaging engines exist which focus near-IR laser beams to diffraction-limited spots²³ of only a few μ m. Comparing Figs. 4, 6 and 8 shows that the imaged spots produced with energetic underlayers are not as round and perfect as in the basic imaging medium, which likely follows from the tearing dynamics of the debonding pro-

cess. Optimization of practical imaging materials with energetic underlayers might involve systematically altering the generation of hot gas-phase decomposition products and the adhesion of the energetic layer to the substrate to produce more ideal spots at lower laser fluences. 

Acknowledgment. This work was supported by a grant from Presstek, Inc. Additional support from the US Army Research Office, through contract No. DAAH04-96-1-0038 is gratefully acknowledged.

References

1. J. M. Sturge, V. Walworth and A. Shepp, *Imaging Processes and Materials*, Van Nostrand Reinhold, New York, 1989.
2. C. DeBoer, Laser thermal media: the new graphic arts paradigm, *J. Imag. Sci. Technol.* **42**, 63 (1998).
3. M. L. Levene, R. D. Scott, and B. W. Stryj, Material transfer recording, *Appl. Opt.* **9**, 2260 (1970).
4. D. Maydan, Micromachining and image recording on thin films by laser beams, *Bell System Tech. J.* **50**, 1761 (1971).
5. R. Goulet and D. Fournier, Workflow as a fundamental motivation for technical evolution, in *IS&T's 49th Annual Conference*, IS&T, Springfield, VA, 1996, p. 469.
6. R. E. Bills, S. C. Busman, W. V. Dower, T. A. Isberg, W. A. Tolbert, D. E. Vogel, M. B. Wolk, and K. A. Zakilika, Study of exothermic laser thermal ablation materials, in *IS&T's 49th Annual Conference*, IS&T, Springfield, VA, 1996, p. 487.
7. D. L. Roberts, USA Patent No. 3,787,210 (1974).
8. R. L. Wilkinson and R. W. Crowell, European patent specification Patent No. 81109245.1 (1986).
9. T. E. Lewis, M. T. Nowak, and K. T. Robichaud, U.S. Patent No. 5,353,705 (1994).
10. R. E. Bills, W. V. Dower, T. A. Isberg, S. C. Busman, J. C. Chang, M. Li, and H. Chou, USA Patent No. 5,278,023 (1994).
11. J. O. H. Peterson, USA Patent No. 3,964,389 (1976).
12. R. I. Oransky and D. G. Savage, USA Patent No. 4,245,003 (1981).
13. J. Sakata and C. Wight, Shock-induced chemistry of energetic materials, *J. Phys. Chem.* **99**, 6584 (1995).
14. Y. Haas, Y. Bel Eliahu, and S. Welner, Infrared laser-induced decomposition of GAP, *Combust. Flame* **96**, 212 (1994).
15. T. E. Lewis, M. T. Nowak, K. T. Robichaud, and K. R. Cassidy, U.S. Patent No. 5,339,737 (1994).
16. D. E. Hare, S. T. Rhea, D. D. Dlott, R. J. D'Amato, and T. E. Lewis, Fundamental mechanisms of lithographic printing plate imaging by near-infrared lasers, *J. Imag. Sci. Technol.* **41**, 291 (1997).
17. S. G. Koulikov and D. D. Dlott, Time-resolved three-dimensional microscopy of laser photothermal imaging processes, in *IS&T's NIP 14: International Conference on Digital Printing Technologies*, IS&T, Springfield, VA, 1998, p. 172.
18. D. E. Hare, S. T. Rhea and D. D. Dlott, New method for exposure threshold measurement of laser thermal imaging materials, *J. Imag. Sci. Technol.* **41**, 588 (1997).
19. D. E. Hare, S. T. Rhea, D. D. Dlott, R. J. D'Amato, and T. E. Lewis, Pulse duration dependence of lithographic printing plate imaging by near-infrared lasers, *J. Imag. Soc. Technol.* **42**, 90 (1998).
20. C. Vovelle, J.-L. Delfau, M. Reuillon, J. Bransier, and N. Laraqui, Experimental and numerical study of the thermal degradation of PMMA, *Combust. Sci. and Technol.* **53**, 187 (1987).
21. D. W. Van Krevelen, *Properties of Polymers*, Elsevier, Amsterdam, 1990.
22. I.-Y. S. Lee, W. A. Tolbert, D. D. Dlott, M. M. Doxtader, D. M. Foley, D. R. Arnold, and E. R. Ellis, Dynamics of laser ablation transfer imaging investigated by ultrafast microscopy, *J. Imag. Sci. Technol.* **36**, 180 (1992).
23. D. Gelbart, High power multi-channel writing heads, in *IS&T's 10th International Congress on Advances in Non-Impact Printing Technologies*, IS&T, Springfield, VA, 1994, p. 337.